Evidence for a Spatiotemporal Singularity in Percept Formation by Cerebral Cortex

Walter J Freeman[1]

[1] Department of Molecular & Cell Biology, University of California at Berkeley, Berkeley CA 94720-3206 USA dfreeman@berkeley.edu

Freeman WJ (2009) Evidence for a spatiotemporal singularity in percept formation by cerebral cortex. In: Adv Cogn. Neurodyn (II): Proc 2nd Int Conf Cogn Neurodyn (eds. Wang R, Gu F), Springer, pp. 585-596.

Abstract. Perception proceeds by cinematic frames that are separated by an endogenous *shutter,* which is intrinsic to the background *spontaneous* activity of cerebral cortex. Cinematic displays of spatiotemporal electrocorticograms (ECoG) show turbulence, from which stable spatial patterns emerge that are correlated with perception of conditioned stimuli (CS). Extracting invariant properties of the perceptual patterns requires high-resolution measurements by high-density electrode arrays, high-order FIR filters, and the Hilbert transform giving analytic signals (instantaneous amplitudes and frequencies). Each pattern is preceded by a *null spike*, which is postulated to reveal a *singularity* in cortical dynamics that operates the shutter. A piecewise linear model is used to solve the nonlinear differential equations of mesoscopic cortical dynamics. Solutions point to the existence of a limit cycle attractor. The behavioral and physiological circumstances are described by which the trajectory of cortical dynamics may converge to the attractor and precipitate a phase transition, which destroys an existing pattern and initiates a new one.

Keywords: AM pattern; electrocorticogram (ECoG); null spike; perceptual frame; phase transition; PM pattern (cone); singularity; vortex

1 Introduction

Sensory cortices in brains sustain the embedding of the self in the environment by organizing sensory information into perceptions that express the meaning and significance of the sensory input. Each batch of sensory input from a saccade, whisk or sniff of a conditioned stimulus (CS) delivers a volley of action potentials to the appropriate sensory cortex. That burst of input helps to trigger a phase transition [18, 23] that condenses a disorderly receiving phase into a widely synchronized, orderly transmitting phase. The order is expressed in a narrow band carrier wave that is modulated in amplitude (AM) and phase (PM) [4, 5, 6]. The AM and PM patterns are fixed within *frames* between phase transitions [7]. The spatial AM pattern is governed by an attractor that is selected by the CS from a landscape of basins of attraction. Its detailed shape is determined by the synaptic connections among cortical neurons in a nerve cell assembly that stores the memory of the CS as a category. That recalled memory is transmitted by the

sensory cortex to other parts of the brain in the form of the AM pattern. The sensory information updates the synaptic connections in the assembly and is then discarded. The spatial PM pattern in the form of a phase cone defines the spatial location and temporal duration of the synchrony.

The hypothesis is proposed [10, 18] that the initiation of a phase transition requires the approach of cortical dynamics to a singularity [17] that is manifested by an extreme event [10, 20, 26] at a *point in time and space*. This extreme event called a *null spike* [10] has been identified as a sudden decrease in the background activity that occupies the spectral band of the induced carrier wave. New data confirm the extreme space-time localization of null spikes that precede the onsets of AM and PM patterns (phase cones). The spatial location of null spike and the apex of the following cone often coincide, but only after optimization of the search parameters and avoidance of overlapping wave bursts. The singularity is explained as a limit cycle attractor [2], which the cortical dynamics approaches in the conjunction of several conditions: high behavioral arousal, an increase in amplitude of cortical activity from a CS, and the approach toward zero in the power of the background filtered ECoG: the null spike. The conjunction increases the signal-to-noise ratio without limit. By the crossing of an as yet ill-defined threshold, a disorderly 'gaseous' receiving phase condenses into an ordered 'liquid' transmitting phase by a phase transition [9].

2 Methods

A. Experimental Methods

ECoG data were recorded from the olfactory bulb and cortex and the visual, auditory and somatic cortices of rabbits that were trained to respond to olfactory, visual, auditory or somatic CS [1]. High resolution was required for measurement of ECoG signals in the spatial, spectral, and temporal dimensions. High *spatial resolution* was optimized by use of spatial spectral analysis to minimize the distance between electrodes (0.79 mm) in square electrode arrays with optimal aperture (6x6 mm) on the cortical surface (Chapter 4 in [2], [11]). High *spectral resolution* was by a FIR filter with order 1000 to 4000 to optimize a pass band of 5 Hz in the beta and gamma ranges [10, 15]. High *temporal resolution* was optimized by sampling at 500/s over time segments lasting 6 sec, which was the duration of individual trials (3 s control period with no CS followed by 3 s with CS) and by use of the Hilbert transform [8]. The *instantaneous analytic signal* was calculated and decomposed into the analytic power (amplitude squared) and the unwrapped analytic phase [4, 5]. The analytic frequency was calculated as a time series by dividing successive analytic phase difference (in radians) by the duration of the digitizing step (here 0.002 s) and by 2π radians/cycle to express the values in Hz.

The power spectral density was calculated with the multitaper window [25] (MATLAB pmtm) and displayed in log-log coordinates. The choice of the order of the filter depended on the digitizing step of 2 ms and the pass band. Empirically

order 500 gave invariance of the distribution of minimal amplitudes in null spikes over the relevant pass bands (Table 1) [15]. The pass bands were calculated in multiples of the Nyquist frequency (100 Hz and 250 Hz) in order to approximate the conventional pass bands, and in order to show the scale-invariance of the oscillations in each pass band, when the duration of display was changed inversely with the frequency range [15].

Table 1. Filter settings based on Nyquist frequency (Nf)

Band	Band pass	2 ms step	5 ms step	display, s
high gamma	50-100 Hz	1/2.5-1.5 Nf	1/2-1 Nf	1
low gamma	25-50 Hz	1/10-1/5 Nf	1/4-1/2 Nf	2
beta	12.5-25 Hz	1/20-1/10 Nf	1/8-1/4 Nf	4
alpha	6.25-12.5 Hz	1/40-1/20Nf	1/16-1/8 Nf	8
theta	3.125-6.25 Hz	1/80-1/40Nf	1/32-1/16 Nf	16

B. Theoretical Methods

The simplest mesoscopic cortical circuit that suffices to model cortical dynamics contains two neural populations that form a KII set [13]: one is an excitatory KIe set; the other is an inhibitory KIi set. The minimal connections require that each KI set be modeled by a positive feedback loop between respectively 2 KOe sets and two KOi sets. The linear part of the KO cortical dynamics is revealed by the non-oscillatory *impulse response* (averaged evoked potential) under deep anesthesia. It can be fitted with the solution of a 2^{nd} order ordinary differential equation (ODE), which is the sum of two exponentials. One term gives the initial rise rate, a = 220/s, and the other term gives the decay rate, b = 720/s, to the pre-stimulus baseline [2].

In the waking, behaving state the impulse response is oscillatory; it is measured by fitting to it the sum of two damped cosines [2, 13]. The power-law distribution of connection density with distance of transmission [12] endows the cortex with the property that, when a phase transition begins, it extends from a site of nucleation over the entire sensory cortex irrespective of its size. The resulting long correlation length makes it feasible to model the transition dynamics with a lumped approximation of the 2-D system. The linear part of the KII set is modeled by four 2^{nd} order ODE [13]. The two rate constants, a and b, are the same for all four KO sets. The nonlinear part of the KII set is modeled by a time-invariant asymmetric sigmoid function at the output of each of the four populations.

The system is piece-wise linearized by replacing the sigmoid curve of each KO set with 1 of 4 fixed gain coefficients that are equal to the slope of the tangent to the sigmoid curve at a given operating point. That point is determined by measurement of the closed loop impulse response. It has the form of the sum of 2 damped cosines. The four interactions of the KII set are expressed in four nonlinear gain

parameters: excitation of excitatory or inhibitory, inhibition of excitatory or inhibitory.

The important parameters from fitting damped cosines to the impulse responses are the amplitude, frequency, ω, and decay rate, α, of the cosine with ω in the gamma range and the value of α that is closest to the $j\omega$ axis. The 4 gain coefficients in the model predict the values of ω, α, amplitude, v, and phase, ϕ, of the impulse response. Conversely, the experimental values of ω, α, v, and ϕ serve to evaluate the 4 gain coefficients in the model.

Sets of solutions are generated to calculate the changes in the impulse responses with changes in the state of the cortex that are expressed in the closed loop poles and zeroes of the linear solutions. The state dependence of cortical dynamics is displayed by the paths of the closed loop poles and zeroes that are generated by changing the cortical state with anesthetics or changing the intensity of the input impulse, $\delta(t)$. These paths are *root loci*. Owing to the symmetry of the upper and lower halves of the complex plane, only the upper half need be displayed. Full details of methods are available on-line [2].

3 Results

A. Experimental Results

The temporal ECoG power spectral density (PSD_T) in coordinates of log power vs. log frequency was calculated over segments relatively long in duration (1 to 6 s). Typically the PSD_T conformed to a power-law (1/f) distribution in three frequency ranges having different slopes (Fig. 1, **A**, black curve). In the range of delta, theta and alpha (<12.5 Hz) the slope tended toward zero ($1/f^0$) but with peaks above the trend line in segments having narrow band oscillations (Fig. 1, A, dark curve). In the range of high beta and most of gamma (12-80 Hz) the slope varied between the limits of -1 to -3 ($1/f^1$ to $1/f^3$) depending on the behavioral state (especially waking vs. sleeping [19]). Above 80 Hz the slope was close to -4 ($1/f^4$) in the absence of noise [24] and to 0 ($1/f^0$) in the presence of noise [16].

The PSD_T of short segments (80-120 ms) extracted with a non-overlapping window stepped across the ECoG revealed multiple peaks coexisting at each step (Fig. 1, **A**, gray curve), which varied in center frequency from each step to the next. The PSD_T was used to decompose the ECoG by centering a narrow band pass filter (5 Hz width) on each peak. The output was an oscillation that waxed and waned in amplitude in correspondence with the formation of bursts in the ECoG at different carrier frequencies. The example shown in Fig. 1, **C**, was from the peak in power in the high gamma range (50-55 Hz). During high power (Fig. 1, B) the spatial pattern of amplitude and the frequency (Fig. 1, D) both were relatively fixed [4] but they both changed from each frame to the next.

Evidence for the mechanism of the change was sought in the amplitude trough of between frames. The trough was visualized by superimposing all available signals (62 channels in Fig. 1). The display worked because all the signals had the same instantaneous frequency with minimal phase dispersion (within $\pm\pi$ rad = ±45°). At one or more time steps the analytic power (**B**, **a**) decreased to very near zero at or near one channel, and the analytic frequency (**D**, **a**) was indeterminate (as manifested by the very high spatiotemporal variance). At that moment there was a discontinuity in the ECoG signal in this pass band that was expressed in phase slip from one pre-existing carrier frequency in a preceding frame to a new carrier frequency in the next succeeding frame on all signals. This event (downward spike in poser, maximum spatial SD_X of the analytic frequency, and analytic phase discontinuity) was inferred to serve as a *temporal marker* for the phase transition.

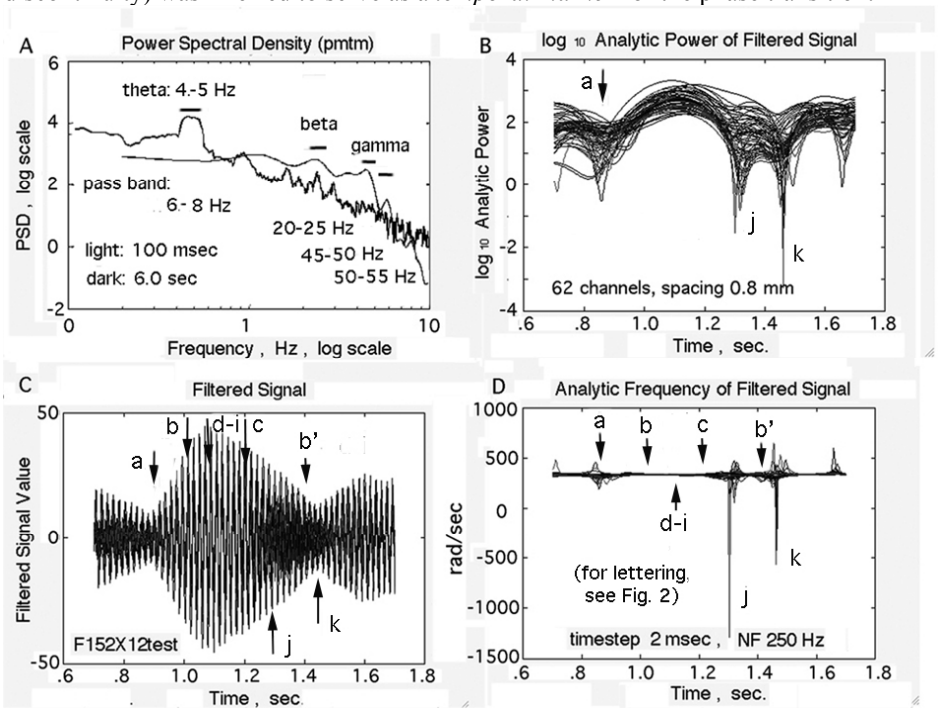

Fig. 1. **A**. PSD_T. Finding the carrier band to within ± 2.5 Hz was crucial [19]. **B**. Gamma ECoG, 62 superimposed signals. **C**. Log_{10} analytic power from the Hilbert transform of band pass filtered signals [8]. **D**. Analytic frequency. Phase resolution needed to demonstrate spatial coincidence of the null spike and the apex of the following conic phase gradient holds only for non-overlapping down spikes (as at **a**) and not when other bursts superimpose (as at **j** and **k**).

A *spatial marker* for the phase transition was revealed by plotting the analytic power as a function of spatial location (Fig. 2). Serial spatial maps of the log_{10} analytic power in the filtered ECoG (the time series in Fig. 1, **C**), when displayed as movies [31], revealed a surface that flapped and rolled like an ocean in storms [18, 23]. Intermittently the power decreased in a brief spike (Fig. 2, **a**). The shape

and width of the spike (Fig. 2, **a**) conformed to the point spread function of a point dipole located at a depth of 1 to 1.5 mm below the recording array on the cortex, which corresponded to the depth of the generating layer of cortical dendrites (Ch. 4 in [2], [7]).

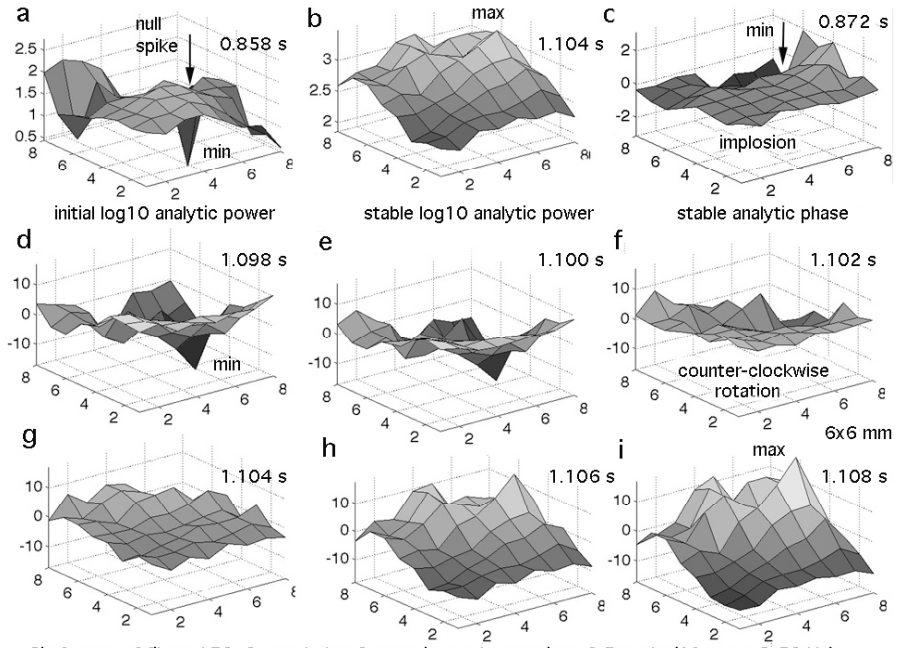

Fig. 2**.** Co-localization was found of the null spike, cone apex, and center of rotation in bursts in which one frequency dominated (Fig. 1, **C**). **a.** The spatiotemporally localized null spike at **a** in Fig. 1 emerged between AM patterns. **b.** The invariant AM pattern of the burst from **b-b′** in Fig. 1 was determined by learning. **c.** The invariant PM pattern in **b-c** in Fig. 1 conformed to an inverted cone. **d-i.** Half cycle ECoG amplitudes at 52 Hz revealed rotation [18, 23].

.

Another type of spatial marker had previously been found by mapping the 64 phase values of the carrier wave at its center frequency with respect to the spatial average phase at each time step [1, 11]. The phase surface formed by the 8x8 array of phase values was fitted with a cone. In roughly half of the cones the apex had phase lead corresponding to an explosive radiation, whereas half had phase lag at the apex (implosion). The location of the apex of a cone was postulated to correspond to the maximum or minimum of phase and to coincide with the location of the preceding null spike. It did so (Fig. 2, **c**) if there was only one dominant frequency in the oscillatory burst (time segment **a** to **b'** in Fig. 1, **C**) but not if the segment contained two components or more (preceding **a** and segment **j** to **k**). It was postulated that two or more superimposed bursts distorted the phase distribution from a cone [5]. Attempts to fit the sum of two cones failed, owing to insufficient information for convergence of nonlinear regression [11].

A third source of evidence for a critical spatial point in the phase transition came from the cinematic display [31] of the filtered ECoG amplitude (Frames **d-i** in Fig. 2). The spatial pattern of the ECoG amplitude in a single half-cycle was sampled from minimum to maximum at 2 msec time steps at the arrow **d-i** in Fig. 1, **C**). The center frequency was 52 Hz; the wavelength was 19 msec, so each half cycle had six 2-msec steps. The successive cinematic frames [31] in this example revealed counterclockwise rotation of the field of ECoG potential around a center point close to the site of the preceding null spike. The field resembled the appearance of a vortex in a satellite image of a hurricane [14, 18]. Other examples revealed clockwise rotation, irrespective of the sign of the phase gradient (negative: explosion: positive: implosion). In contrast, the normalized spatial pattern of the analytic power (Fig. 2, **b**) was constant across the half cycle and in fact across the time segment **b** to **c** in Fig. 1, **B**. Collocation of the center of rotation with the null spike preceding the frame was not observed unless there was only one dominant frequency of oscillation carrying a spatial AM pattern.

B. Theoretical Results

The solutions to the piece-wise linear approximation of cortical dynamics by four 2^{nd} order ODE generated 8 poles. Of the 8 poles the only pair of importance was the complex conjugate pole pair closest to the imaginary axis of the complex plane, and then only if the root loci crossed the imaginary jω axis. Owing to the symmetry of the complex pole pair, $-\alpha \pm j\omega$, the display of the root locus plot was restricted to the upper half of the complex plane in the frequency range of $\omega = 0$ to 400 rad/s (64 Hz) and decay rate $\alpha = -200$/s to +100/s. The graph showed a family of root loci. Each locus running mainly down and rightward showed the decreases in (ω, α) with increasing response amplitude (shown by the tick marks). The increase in amplitude imposed a concomitant increase in negative feedback gain, as predicted from the sigmoid nonlinearity (Ch. 3 in [2], [13]). The group of root loci (stacked from left to right) showed the increase in frequency and amplitude with increase in the steepness of the sigmoid curve with the degree of arousal (Ch. 5 in [2]), resulting in increased forward gain.

The conditional instability of the cortex indicating the possibility of a phase transition was predicted by the crossing of the group of root loci over the imaginary axis. The upper crossing was from left to right (conversion of the sign of the real part, α, of the root was from – to +) with increasing forward gain and negative feedback gain. The crossing predicted that response amplitude would continue to increase and carry the system into an exponential increase in oscillatory amplitude: a burst. However, the root loci turned to the left and crossed back into the left of the jw axis. The convergence indicated an approach to a limit cycle attractor, because further increase in amplitude would increase the decay rate, a, and thereby decrease the feedback gain. This piecewise linear analysis provided a scaffold for using the impulse response to demonstrate the relation between degree of stability

of the cortex modeled by the KII set in relation to arousal, sensitization by learning forming Hebbian assemblies for CS [6], and the predicted frequencies of bursts.

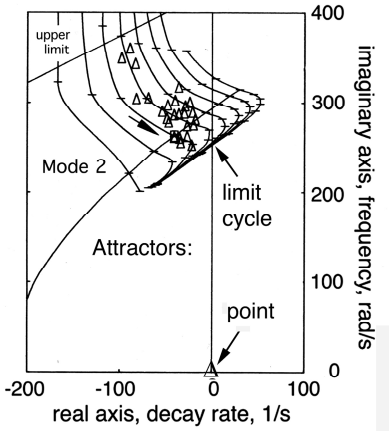

Fig. 3. The plot symbols Δ show the frequency, ω, and decay rate, α, of the damped cosine fitted to the impulse response of the olfactory cortex. The cluster of points came from a set of responses at fixed input intensity; the variation reflects the fluctuations in the level of the background activity. The curves represent a family of root loci, which show the direction of decrease in frequency and decay rate (arrow downward to the right) with increase in response amplitude. The two attractors are inferred to govern the cortical dynamics. From [2, p. 374, Fig. 6.21 (a)].

What remained to be explained sorted out was the sources of the spontaneous variation. The group of root loci could be explained by fluctuations in arousal, including the trend in each experimental data set for reduced arousal from satiety and fatigue. The orthogonal variation along each root locus in the group was replicated by giving sufficient anesthetic to reduce the background activity to a low level and then augmenting it by tetanic stimulation (high-frequency electrical stimulation, e.g., 200 Hz) of the incoming axons to the sensory cortex. This artificial noise temporarily reversed the effect of the anesthetic by increasing the frequency of oscillation and the decay rate over the physiological beta and gamma ranges (Fig. 4). Therefore the spontaneous variation was at least in part attributed to the fluctuations in the background Rayleigh noise in the filtered ECoG, including the down spikes. In brief, the location of the operating point of the cortex as revealed by the frequency and decay rate of the impulse response was dependent on arousal and on the signal-to-noise ratio of the CS-induced signal to the intrinsic, self-organized background spontaneous noise.

4 Discussion

The proposed hypothesis is that the phase transition that initiates each new frame in perception is dependent on a singularity in cortical dynamics. The key experimental evidence is the null spike, which has been discovered by pushing to the limits of the spatial, temporal and spectral resolution of ECoG. Experimentally

the singularity resides in a spatiotemporal point, which does not conform to a pontifical neuron or to a cortical column but to a unique point in a vector field of mesoscopic activity [14]: the null spike; the conic apex; the center of rotation. The key theoretical evidence comes from the group of root loci fin the piecewise linear analysis of the KII set. The onset of instability is marked by the sign reversal (- to +) of the real part, a, of the complex pole pair, $-\alpha \pm j\omega$, with increasing amplitude. The singularity is modeled by the convergence of the root loci where they converge to the $j\omega$ axis and $\alpha = 0$. It occurs when the operating point approaches the limit cycle attractor, where the amplitude predicted from linear approximation increases exponentially, the background noise approaches 0, and the signal-to-noise ratio approaches ∞.

A. A proposed neural mechanism of the null spike

The first question for discussion is how the null spike is generated. The answer is found in conceiving the background activity in the rest state as band-limited noise that generates beats: Rayleigh noise. The background ECoG has been shown to be close to brown noise, for which the PSD_T is power-law with a slope = -2 ($1/f^{\varepsilon}$, ε = 2). That would hold only for the output of an ideal random source that was free of other kinds of noise. The power-law PSD_T of ECoG was found to have slopes that were closer to -3 (*black noise*). That deviation from the ideal was shown to be due to the intrinsic stabilization of the level of the background by the refractory periods [19] that decreased power in the PSD_T in proportion to the square of the frequency.

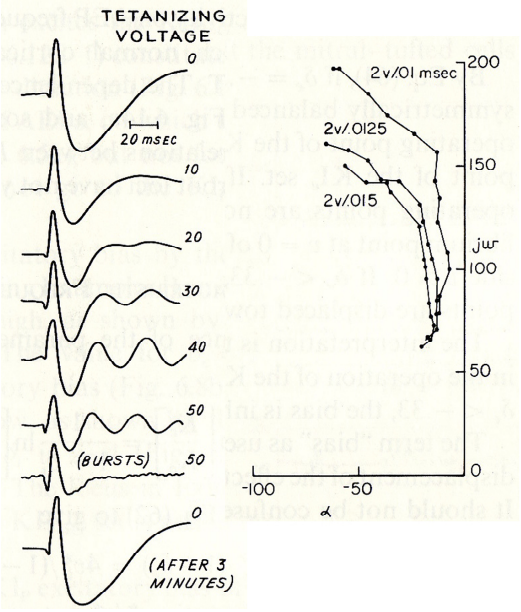

Fig. 4. On the left are examples of impulse responses (averaged evoked potentials) from the cat olfactory cortex. The background was suppressed by anesthesia and then replaced by tetanizing the axons. The frequency, w, and decay rate, a, increased in proportion to the intensity of the background activity, showing that the stability of cortex was reduced

(decrease in decay rate) by the decrease in the background level, putatively resulting from the spontaneous occurrence of down spikes. From [2, p. 365, Fig. 6.13-4]

The form of the impulse response (the damped cosine) implied that in the awake cortex showed that the negative feedback interactions between the excitatory and inhibitory populations operated as a band pass filter, which revealed the characteristic frequencies in the beta and gamma ranges, because that perturbation, $\delta(t)$, contained all frequencies. The action of this intrinsic filter on the background activity in active states was seen in the oscillatory bursts and peaks in the PSD_T at high temporal resolution of the spectrum (Fig. 1, **A**). In the absence of input the endogenous oscillations were indistinguishable from the broad spectrum of black noise. The filtering action of the KII negative feedback that was simulated by applying band pass filters to the ECoG gave Rayleigh noise. The action of the negative feedback on the intrinsic oscillations evoked by sensory input was to give Rice noise [28], for which the intervals between beats were up to twice as long as those for Rayleigh noise. The null spikes occur as beats between the bursts [10].

By experiment [10] and theory [28] the modal interval between down spikes was a function solely of the bandwidth at all center frequencies. The modal interval that conformed to the repetition rate of bursts in the theta range (3-7 Hz) predicted the optimal pass band of 5 Hz. This value was confirmed experimentally. The bandwidth of the KII negative feedback was estimated from the minimal spatial standard deviation (SD) of the analytic frequency in each frame [10].

The distribution of the magnitudes of the down spikes in the rest state was random, because it conformed to that of spikes in filtered black noise [15]. Deviations from randomness in distribution from the active state appeared as excesses and deficits from values predicted for random noise [15, 20]. The modal interval between bursts that had classifiable AM patterns suggested that the threshold for reduction in power in the null spikes that would incur phase transitions was $\sim 10^{-4}$ below the modal power [15].

B. Interpretation of the role of the null spike in perception

These diverse findings give a testable hypothesis of how the enormous neural population in a sensory cortex might transform itself from each frame to the next in an eye blink, destroying a pre-existing pattern, and initiating a new one that conveys a meaningful perception based on current sensory information. The key to interpretation is to consider the ECoG not as an electric potential but as an order parameter [21], that is, as an *index* of the strength of mesoscopic interactions among a cortical population. That interaction enables a sensory cortex to integrate its sensory information with its past experience and create an active memory that drives behavior. The ECoG order parameter is a vector that is evaluated by the AM pattern in each frame [14, 17].

The mass action that results from interaction must be sufficiently powerful to exert its influence on large populations elsewhere in the brain. This is ensured by the

global synchrony of simultaneous transmission by virtually all of the projection neurons in the cortex and by a spatial integral transformation that is performed by a divergent-convergent topology in the pathway carrying cortical output [12]. Further evidence for the repetitive framing of brain activity patterns has been found recently through extension of the search for synchronized amplitude and phase patterns from the intracranial ECoG to the scalp EEG [26, 27, 29].

Pursuit of this speculative hypothesis will require both experimental and theoretical advances. The main experimental deficiency is that the null spike usually fails to coincide with two other singular values: the apex of a conic phase distribution and the center of rotation of a vector field. The failure can be ascribed to several factors, including undersampling the spatial and temporal data streams, inadequate and inaccurate spatial and temporal decomposition of the AM and PM patterns, and lack of robust descriptions of null spikes, which often appear to move in their brief lifespan, which occur in clusters that are analogous to tornado vortices in weather systems [14, 18], and which are too brief to detect rotation at existing digitizing rates.

The main theoretical deficiency is the lack of mathematical structure linking the basic physics of singularities in vector fields with the electrophysiological data, with linear control systems in electrical engineering, and with the theory of behavior. Three behavioral factors determine the approach of the operating point along a root locus to the attractor that expresses the dynamic of phase transition. One is arousal contributing to the signal amplitude (Fig. 3) and the background noise level (Fig. 4). The second is the input-dependent amplification of the impulse response by the sigmoid nonlinearity. The third is the selective sensitivity to a CS that depends on formation of a Hebbian cell assembly through learning. The concept of singularity is proposed here to indicate a fruitful direction [30] in which to explore a major question in contemporary neuroscience: how do we perceive?

References

1. Barrie JM, Freeman WJ, Lenhart M.] (1996) Modulation by discriminative training of spatial patterns of gamma EEG amplitude and phase in neocortex of rabbits," J Neurophysiol 76: 520-539.
2. Freeman WJ (1975/2004) Mass Action in the Nervous System. New York: Academic Press. For the singularity, see equations in Ch. 6 and summary Fig. 6.30 on page 388. http://sulcus.berkeley.edu/MANSWWW/MANSWWW.html
3. Freeman WJ (1990) On the problem of anomalous dispersion in chaoto-chaotic phase transitions of neural masses, and its significance for the management of perceptual information in brains. Chapter in: Haken H, Stadler M (eds.) Synergetics of Cognition. Berlin, Springer-Verlag, Vol 45: 126-143.
4. Freeman WJ (2004) Origin, structure, and role of background EEG activity. Part 1. Analytic amplitude. Clin Neurophysiol 115: 2077-2088.
5. Freeman WJ (2004) Origin, structure, and role of background EEG activity. Part 2. Analytic phase. Clin Neurophysiol 115: 2089-2107.
6. Freeman WJ (2005) Origin, structure, and role of background EEG activity. Part 3. Neural frame classification. Clin Neurophysiol 116/5: 1118-1129.

7. Freeman WJ (2006) Origin, structure, and role of background EEG activity. Part 4. Analytic phase. Clin Neurophysiol 117/3: 572-589.
8. Freeman WJ (2007) Hilbert transform for brain waves. Scholarpedia 2(1): 1338
9. Freeman WJ (2008) A pseudo-equilibrium thermodynamic model of information processing in nonlinear brain dynamics. Neural Networks 21: 257-265. http://repositories.cdlib.org/postprints/2781
10. Freeman WJ (2009) Deep analysis of perception through dynamic structures that emerge in cortical activity from self-regulated noise. Cognitive Neurodynamics 3(1): 105-116.
11. Freeman WJ, Baird B (1987) Relation of olfactory EEG to behavior: Spatial analysis: Behav Neurosci 101: 393-408.
12. Freeman WJ, Breakspear M (2007) Scale-free neocortical dynamics. Scholarpedia 2(2): 1357.
13. Freeman WJ, Erwin H (2008) Freeman K-set. Scholarpedia 3(2): 3238.
14. Freeman WJ, Kozma R (2010) Freeman's mass action. Scholarpedia 5(1):8040
15. Freeman WJ, O'Nuillain S, Rodriguez J (2008) Simulating cortical background activity at rest with filtered noise. J Integr Neurosci 7(3): 337-344.
16. Freeman WJ, Rogers LJ, Holmes MD, Silbergeld DL (2000) Spatial spectral analysis of human electrocorticograms including the alpha and gamma bands. J Neurosci Methods 95: 111-121.
17. Freeman WJ, Vitiello G (2006) Nonlinear brain dynamics as macroscopic manifestation of underlying many-body field dynamics. Physics of Life Reviews 3: 93-118.
18. Freeman WJ, Vitiello G (2009) Dissipative neurodynamics in perception forms cortical patterns that are stabilized by vortices. J. Physics Conf Series **174**(2009)012011.
19. Freeman WJ, Zhai J (2009) Simulated power spectral density (PSD) of background electrocorticogram (ECoG). Cognitive Neurodynamics 3(1): 97-103.
20. Freyer F, Aquino K, Robinson PA, Ritter P, Breakspear M (2009) Bistability and non-gaussian fluctuations in spontaneous cortical activity. J Neurosci 29(26): 8512– 8524.
21. Haken H (1991) Synergetic Computers & Cognition. Berlin: Springer.
22. Izhikevich E, Edelman G (2008) Large-scale model of mammalian thalamocortical systems. PNAS 105 (9): 3593-3598.
23. Kozma R, Freeman WJ (2008) Intermittent spatio-temporal de-synchronization and sequenced synchrony in ECoG signals. Chaos 18:037131.
24. Miller KJ, Sorenson LB, Ojemann JG, den Nijs M (2009) Power-law scaling in the brain surface electric potential. PLOS Comp. Biol. 5(12): e1000609. doi:10.1371/journal.pcbi.1000609
25. Percival DB, Walden AT (1993) Spectral Analysis for Physical Applications: Multitaper and Conventional Univariate Techniques. Cambridge UK: Cambridge UP.
26. Pockett S, Bold GEJ, Freeman WJ [2009] EEG synchrony during a perceptual-cognitive task: Widespread phase synchrony at all frequencies. Clin Neurophysiol 120: 695-708. doi:10.1016/j.clinph.2008.12.044
27. Pribram K (2007) Holonomic brain theory. Scholarpedia, 2(5):2735.
28. Rice SO (1950) Mathematical Analysis of Random Noise - and Appendixes – Technical Publications Monograph B-1589. New York: Bell Telephone Labs Inc. Sect. 3.8., page 90, equ. 3.8-15.
29. Ruiz Y, Li G, Freeman WF, Gonzalez E. [2009] Detecting stable phase structures on EEG signals to classify brain activity amplitude patterns. J Zhejiang Univ 10(10): 1483-1491.
30. Vitiello G [2001] My Double Unveiled. Amsterdam: John Benjamins.
31. http://sulcus.berkeley.edu/Null_Spikes_Movies